



This is the accepted manuscript made available via CHORUS. The article has been published as:

Effect of doping on the phase stability and
superconductivity in math

$\text{La}_{1-x}\text{H}_x\text{MnO}_3$

Zepeng Wu, Yang Sun, Artur P. Durajski, Feng Zheng, Vladimir Antropov, Kai-Ming Ho, and
Shunqing Wu

Phys. Rev. Materials **7**, L101801 — Published 27 October 2023

DOI: [10.1103/PhysRevMaterials.7.L101801](https://doi.org/10.1103/PhysRevMaterials.7.L101801)

Effect of doping on the phase stability and Superconductivity in LaH₁₀

Zepeng Wu¹, Yang Sun^{1*}, Artur P. Durajski², Feng Zheng¹, Vladimir Antropov^{3,4}, Kai-Ming Ho⁴,
Shunqing Wu^{1*}

¹*Department of Physics, Xiamen University, Xiamen 361005, China*

²*Institute of Physics, Czestochowa University of Technology, Ave. Armii Krajowej 19, 42-200
Czestochowa, Poland*

³*Ames National Laboratory, Ames, Iowa 50011, USA*

⁴*Department of Physics, Iowa State University, Ames, Iowa 50011, USA*

Abstract

We present a computational investigation into the effects of chemical doping with 15 different elements on phase stability and superconductivity in the LaH₁₀ structure. Most doping elements were found to induce softening of phonon modes, enhancing electron-phonon coupling and improving critical superconducting temperature while weakening dynamical stability. Unlike these dopants, Ce was found to extend the range of dynamical stability for LaH₁₀ by eliminating the van Hove singularity near the Fermi level. The doped compound, La_{0.75}Ce_{0.25}H₁₀, maintains high-temperature superconductivity. We also demonstrate that different Ce doping configurations in the LaH₁₀ structure have a minimal effect on energetic stability and electron-phonon coupling strength. Our findings suggest that Ce is a promising dopant to stabilize LaH₁₀ at lower pressures while preserving its high-temperature superconductivity.

¹ Email: yangsun@xmu.edu.cn (Y.S.) and wsq@xmu.edu.cn (S.W.)

25 □. INTRODUCTION

26 In recent years, it has been experimentally observed that H-rich compounds can exhibit high-
27 temperature superconductivity (HTS) under high pressure, such as H₃S ($T_c = 203\text{K}$ at 155GPa [1]),
28 LaH₁₀ (~250K at 170GPa [2]; ~260K at 180-200GPa [3]), CaH₆ (215K at 172GPa [4,5]), CeH₁₀ (115K
29 at 95GPa [6]), CeH₉ (~100K at 130GPa [6]), (LaCe)H₉ (148-178K at 97-172GPa [7,8]), YH₉ (243K
30 at 201GPa [9-11]), YH₆ (~220K at 183GPa [9]), (LaY)H₁₀ (253K at 183GPa [12]) and LaBeH₈ (110K
31 at 80GPa [13]). These discoveries have set a milestone in approaching the room-temperature
32 superconductivity [14-19]. At the same time, the pressure required to stabilize these compounds is still
33 too extreme for practical applications.

34 The search of binary hydrides [20,21] has shown diverse structures and chemistry in these
35 compounds, which provide a broad platform to optimize the energetic stability and superconductivities.
36 Compared with the binary phases, the ternary phases have a much broader configurational space,
37 thereby offering more possibility for HTS at lower pressures [22]. It has been proposed that replacing
38 H with small-radius elements (such as Be, B, C, N, and Si) can lower the required high pressures in
39 the hydrides [23]. For instance, KB₂H₈ (134K-146K at 12GPa [24]), BaSiH₈ (71K at 3GPa [25]),
40 LaBH₈ (126K at 50GPa [26]), KPb(BC)₆ (88K at ambient pressure [27]), Al₂(BN)₆ (72K at ambient
41 pressure [28]), etc. While these dopants extend the pressure range of the stability, their superconducting
42 temperature is simultaneously reduced.

43 Since the superconductivity in hydrides is mainly due to H, doping on the metal site is likely to
44 maintain its superconductivity. Recently, high-throughput screening in the MgB₂-like systems shows
45 that the doping on the metal site can effectively improve the stability and maintain the
46 superconductivity [29]. Metals from the same family share similar characteristics, allowing them to be
47 combined into disordered solid mixtures. This property allows us to use binary compounds as
48 foundational blueprints for crafting ternary alloy super hydrides from the original crystal structure [30-
49 33]. LaH₁₀, with the highest T_c among experimentally synthesized superconductors, is a potential
50 parent structure for doping to manipulate its HTS and pressure-dependent stability.

51 In this paper, based on first-principles calculations, we investigate the effects of chemical doping
52 on phase stability and superconductivity in the LaH₁₀ structure. A total of 15 elements are selected as
53 dopants: K, Rb, Cs, Ca, Sr, Ba, Sc, Y, Ti, Zr, Hf, In, Tl, Ce, and Lu. The first thirteen elements are
54 more likely to donate electrons to H atoms to enhance the stability of the H cage framework, and the
55 strong correlation effect caused by d electrons is not significant [21]. Ce and Lu have also been
56 theoretically predicted to have good superconducting potential [34,35]. We will use the La_{0.75}M_{0.25}H₁₀
57 model to examine their dynamical stability and superconductivity under high pressure.

58 □. COMPUTATION METHODS

59 2.1 Stability calculations

60 The $\text{La}_{0.75}\text{M}_{0.25}\text{H}_{10}$ structure was constructed by replacing one La atom with M metal (M=K, Rb,
61 Cs, Ca, Sr, Ba, Sc, Y, Ti, Zr, Hf, Ce, Lu, In, Tl) in the conventional cell (four formula units (f.u.))
62 shown in Fig. 1(a). This results in a symmetry reduction to Pm-3m. Structure relaxations and electronic
63 properties were carried out using the Perdew-Burke-Ernzerhof (PBE) [36] functional in the framework
64 of the projector augmented wave (PAW) method [37] as implemented in the VASP code [38]. The
65 configurations of valence electrons used in the PAW method are shown for these elements in Table.
66 S1. A plane-wave basis set with an energy cutoff of 500 eV and uniform Γ -centered k-point grids with
67 a density of $2\pi \times 0.025\text{\AA}^{-1}$ were employed in the self-consistent calculations and structure
68 relaxations. The structures were optimized until the maximum energy and force were less than
69 10^{-8} eV and 1 meV/ \AA , respectively.

70 To investigate the dynamical stability, we used the finite displacement method by constructing a
71 supercell with ~ 352 atoms and uniform Γ -centered k-point grids with a density of $2\pi \times 0.025\text{\AA}^{-1}$.
72 The second-order force constant extraction and the harmonic phonon dispersion relationship
73 calculation were performed with Phonopy code [39]. We employed quasi-harmonic approximation
74 (QHA) to explore the finite temperature thermodynamics.

75 2.2 Electron-phonon coupling calculations

76 Harmonic phonon dispersion and electron-phonon coupling (EPC) were calculated within the
77 density functional perturbation theory (DFPT) [40], as implemented in the QUANTUM ESPRESSO
78 package [41,42]. Ultrasoft pseudopotentials [43] with PBE functional were used with a kinetic energy
79 cutoff of 80 Ry and a charge density cutoff of 800 Ry. The valence electron configurations used in
80 USPP were the same as in PAW potential, so the calculations performed with QE and VASP were
81 consistent. Self-consistent electron density and EPC were calculated by employing $8 \times 8 \times 8$ k-point
82 meshes and $4 \times 4 \times 4$ q-point meshes. A dense $16 \times 16 \times 16$ k-point mesh was used for evaluating electron-
83 phonon interaction matrix.

84 The main input element to the Eliashberg equations is the Eliashberg spectral equation $\alpha^2 F(\omega)$
85 defined as[44,45]

$$86 \quad \alpha^2 F(\omega) = \frac{1}{2\pi N(E_F)} \sum_{qv} \frac{\gamma_{qv}}{\hbar\omega_{qv}} \delta(\omega - \omega_{qv}) \quad (1)$$

87 where $N(E_F)$ is the states at the Fermi level E_F , ω_{qv} representative the phonon frequency of the
88 mode v with wave vector q . The phonon linewidth γ_{qv} , which is the imaginary part of the phonon self-

89 energy, is defined as

$$90 \quad \gamma_{qv} = \frac{2\pi\omega_{qv}}{\Omega_{B.Z}} \sum_{i,j} \int d^3k |g_{k,qv}^{i,j}|^2 \delta(\varepsilon_{i,q} - E_F) \delta(\varepsilon_{j,k+q} - E_F) \quad (2)$$

91 $g_{k,qv}^{i,j}$ is the EPC matrix element, and $\Omega_{B.Z}$ is the volume of the Brillouin zone (B.Z.). The EPC
92 constant is calculated by

$$93 \quad \lambda = \sum_{qv} \frac{\gamma_{qv}}{\pi\hbar N(E_F)\omega_{qv}^2} = 2 \int_0^\infty \frac{\alpha^2 F(\omega)}{\omega} d\omega \quad (3)$$

94 We chose the gaussian smearing width of 0.02-0.03 Ry based on the convergence test in [Supplementary](#)
95 [Note 1 \[46\]](#). T_c was first estimated using McMillan-Allen-Dynes (MAD) formula [44,45] with
96 Coulomb pseudopotential $\mu^* = 0.13$ [47,48].

$$97 \quad T_c = \frac{f_1 f_2 \omega_{log}}{1.2} \exp\left(-\frac{1.04(1+\lambda)}{\lambda - \mu^*(1+0.62\lambda)}\right) \quad (4)$$

98 where f_1 and f_2 are two separate correction factors [44], which are functions of λ , ω_{log} , ω_2 , and
99 μ^* . The logarithmic average frequency ω_{log} is computed as:

$$100 \quad \omega_{log} = \exp\left(\frac{2}{\lambda} \int_0^\infty \frac{\alpha^2 F(\omega)}{\omega} \ln\omega d\omega\right) \quad (5)$$

101 2.3 Migdal-Eliashberg approach

102 The thermodynamic properties of superconducting ternary $\text{La}_{0.75}\text{M}_{0.25}\text{H}_{10}$ hydrides were also
103 estimated using the Migdal-Eliashberg (ME) approach due to the strong electron-phonon coupling
104 constants observed in these systems. The isotropic Eliashberg equations defined on the imaginary-
105 frequency axis, which incorporate the superconducting order parameter function $\varphi_n = \varphi(i\omega_n)$ and
106 the electron mass renormalization function $Z_n = Z(i\omega_n)$ take the following form [49,50]:

$$107 \quad \varphi_n = \frac{\pi}{\beta} \sum_{m=-M_f}^{M_f} \frac{\lambda_{n,m} - \mu^* \theta(\omega_c - |\omega_m|)}{\sqrt{\omega_m^2 Z_m^2 + \varphi_m^2}} \varphi_m, \quad (6)$$

$$108 \quad Z_n = 1 + \frac{1}{\omega_n} \frac{\pi}{\beta} \sum_{m=-M_f}^{M_f} \frac{\lambda_{n,m}}{\sqrt{\omega_m^2 Z_m^2 + \varphi_m^2}} \omega_m Z_m, \quad (7)$$

109 where $\beta = 1/k_B T$, and the electron-phonon interaction pairing kernel is given by,

$$110 \quad \lambda_{n,m} = 2 \int_0^\infty \frac{\omega}{(\omega_n - \omega_m)^2 + \omega^2} \alpha^2 F(\omega) d\omega. \quad (8)$$

111 Hence, the superconducting order parameter was defined by the ratio $\Delta_n = \varphi_n/Z_n$ and the
112 superconducting transition temperature T_c was estimated from the following relation $\Delta_{n=1}(\mu^*, T =$

113 $T_c) = 0$. We used the same Coulomb pseudopotential as the one used in MAD calculations, i.e.,
114 $\mu^*=0.13$. The Eliashberg equations were solved iteratively in a self-consistent way with a maximal
115 error of 10^{-10} between two successive iterations. The convergence was controlled by the sufficiently
116 high number of Matsubara frequencies: $\omega_n = (\pi/\beta)(2n - 1)$, where $n = 0, \pm 1, \pm 2, \dots, \pm M_f$ and
117 $M_f = 1100$ [51-53].

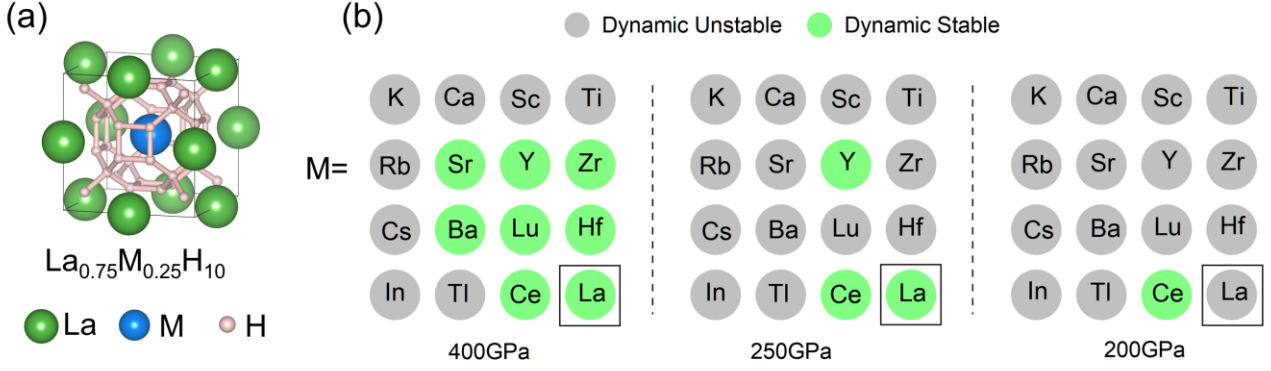
118

119 □. RESULTS AND DISCUSSION

120 3.1 Phase stability

121 We first evaluate the dynamical stability of ternary $\text{La}_{0.75}\text{M}_{0.25}\text{H}_{10}$ structures. Harmonic phonon
122 dispersions were calculated for all 16 phases at 400GPa, 250GPa, and 200GPa (see [Supplementary](#)
123 [Fig. S5 \[46\]](#)). A phase without any imaginary modes in the phonon spectrum is marked as dynamically
124 stable in Fig. 1(b). At 400 GPa, the structure is stable with seven substitutions, i.e., Sr, Ba, Y, Zr, Hf,
125 Ce, and Lu. Y and Ce substitutions can maintain stability when the pressure is reduced to 250 GPa. At
126 200 GPa, only $\text{La}_{0.75}\text{Ce}_{0.25}\text{H}_{10}$ remains stable at harmonic level. LaH_{10} becomes harmonic dynamically
127 unstable below 230 GPa (see Fig. S6). Therefore, Ce substitution can improve the stability of LaH_{10}
128 and lower the pressure range of the stability. Our calculations were based on the harmonic
129 approximation, while the anharmonic effect and the quantum nuclear effect (QNE) were ignored. The
130 anharmonic oscillations of the hydrogen sublattice can contribute to the T_c and thermodynamic
131 stability of hydrides [54-57]. The calculations with QNE and anharmonic correction indicate the LaH_{10}
132 can be stabilized as low as ~ 130 GPa [54,58], similar to the experimental observation at ~ 140 GPa
133 [59]. Therefore, the pressure stability range of present $\text{La}_{0.75}\text{Ce}_{0.25}\text{H}_{10}$ is expected to expand further by
134 including anharmonic and QNE effects.

135 Given the harmonic dynamical stability, we evaluate the thermodynamic stability of
136 $\text{La}_{0.75}\text{Ce}_{0.25}\text{H}_{10}$. We calculated its enthalpy on the ternary phase diagram at 200 GPa, as shown in Fig.
137 S2(a) [46]. The results show that the energy of the $\text{La}_{0.75}\text{Ce}_{0.25}\text{H}_{10}$ structure is only 1 meV/atom higher
138 than that of the convex hull. In addition, we also considered finite temperature thermodynamics (see
139 [Supplementary Note 2 \[46\]](#)) and found the of $\text{La}_{0.75}\text{Ce}_{0.25}\text{H}_{10}$ (Pm-3m) has promising thermodynamic
140 stability up to 300 K.



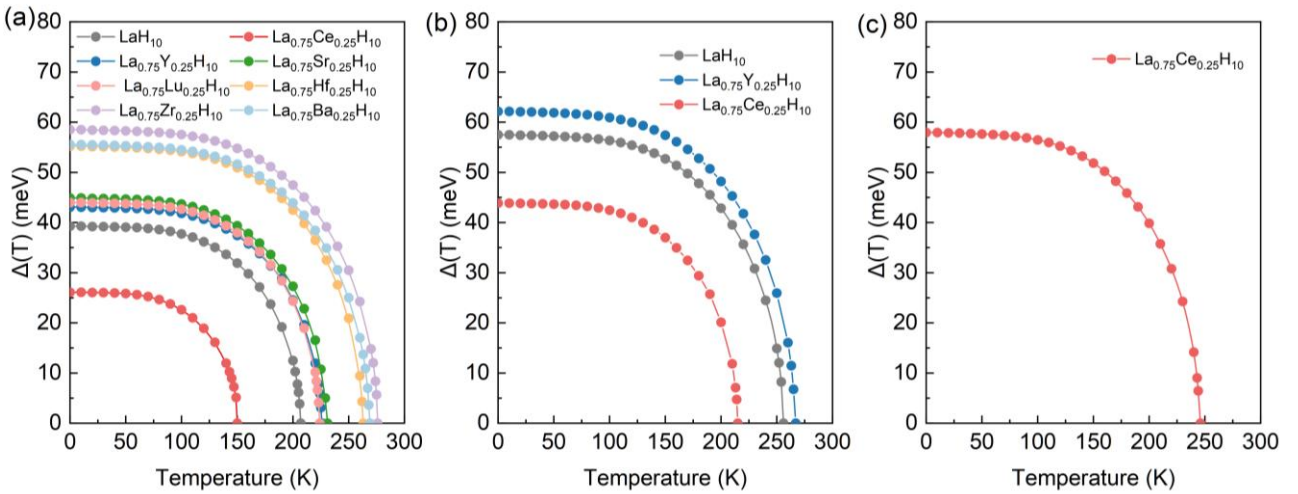
141

142 Fig. 1. (a) Structure of $\text{La}_{0.75}\text{M}_{0.25}\text{H}_{10}$, $\text{M}=\text{K}, \text{Rb}, \text{Cs}, \text{Ca}, \text{Sr}, \text{Ba}, \text{Sc}, \text{Y}, \text{La}, \text{Ti}, \text{Zr}, \text{Hf}, \text{In}, \text{Tl}, \text{Ce}, \text{Lu}$.

143 (b) Dynamic stability of all doped phases at 400 GPa, 250 GPa, and 200 GPa.

144 3.2 Electron-phonon coupling and superconductivity

145 We calculate the EPC constant λ using the DFPT method and Eliashberg theory for the
 146 dynamically stable structures at 400, 250, and 200 GPa. We first compute the superconducting
 147 transition temperature (T_c) by the MAD formula, presented in Table 1. Due to the large λ (>2) in these
 148 compounds, we also employ Eliashberg formalism to investigate the impact of EPC on the T_c and
 149 superconducting energy gap. The temperature-dependent behavior of the superconducting energy gap
 150 $\Delta(T)$ is computed by solving the ME equations in the mixed representation (defined simultaneously
 151 on the imaginary and real axis) [60,50]. The results are presented in Fig. 2, which illustrates the
 152 calculated $\Delta(T)$ curves for dynamically stable structures of $\text{La}_{0.75}\text{M}_{0.25}\text{H}_{10}$ at 400 GPa.



153

154 Fig. 2. Superconducting energy gap as a function of temperature for $\text{La}_{0.75}\text{M}_{0.25}\text{H}_{10}$ at (a) 400 GPa, (b)
 155 250 GPa, and (c) 200 GPa.

156

157 Based on $\Delta(T)$ results, we estimate T_c and compare it with MAD results in Table 1. T_c is found

158 to be high for all investigated cases and reaches the highest value of 276 K for $\text{La}_{0.75}\text{Zr}_{0.25}\text{H}_{10}$ at 400
159 GPa and 267 K for $\text{La}_{0.75}\text{Y}_{0.25}\text{H}_{10}$ at 250 GPa. The T_c values of $\text{La}_{0.75}\text{M}_{0.25}\text{H}_{10}$ predicted via the MAD
160 formula are consistently lower (underestimated) than those obtained from the ME formalism,
161 particularly for the one with large λ . This justifies the usage of the ME formalism: we assumed an
162 underestimation of T_c in the MAD method using the strong coupling ME method. The obtained
163 results entirely confirm the assumption. The calculation of LaH_{10} shows that λ is 2.53 and T_c is 256
164 K at 250 GPa by ME equation. As a reference, the experimental T_c of LaH_{10} was observed at $\sim 250\text{K}$
165 under 170-200 GPa. Therefore, our calculation of T_c is consistent with the experimental data. Below,
166 we use T_c from ME formalism for further analysis.

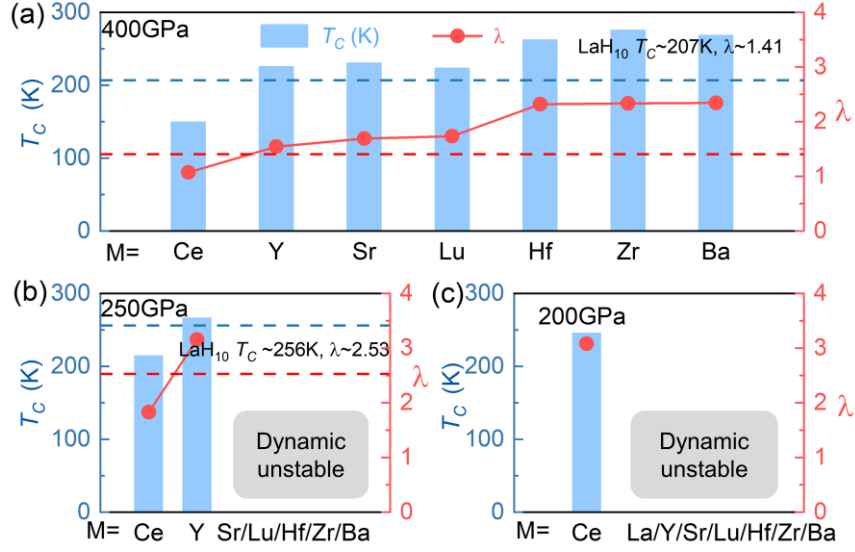
167

168 TABLE □. Superconducting critical temperature (T_c) of dynamically stable $\text{La}_{0.75}\text{M}_{0.25}\text{H}_{10}$ at 200, 250,
169 and 400GPa estimated using Migdal-Eliashberg approach T_{c_ME} .and MAD formula T_{c_MAD}

P(GPa)	Structure	λ	T_{c_ME} (K)	T_{c_MAD} (K)
200	$\text{La}_{0.75}\text{Ce}_{0.25}\text{H}_{10}$	3.08	246	209
	LaH_{10}	2.53	256	220
250	$\text{La}_{0.75}\text{Ce}_{0.25}\text{H}_{10}$	1.83	215	186
	$\text{La}_{0.75}\text{Y}_{0.25}\text{H}_{10}$	3.16	267	208
	LaH_{10}	1.41	207	174
	$\text{La}_{0.75}\text{Ce}_{0.25}\text{H}_{10}$	1.07	150	125
400	$\text{La}_{0.75}\text{Y}_{0.25}\text{H}_{10}$	1.55	226	188
	$\text{La}_{0.75}\text{Sr}_{0.25}\text{H}_{10}$	1.69	231	186
	$\text{La}_{0.75}\text{Lu}_{0.25}\text{H}_{10}$	1.73	224	181
	$\text{La}_{0.75}\text{Hf}_{0.25}\text{H}_{10}$	2.32	263	190
	$\text{La}_{0.75}\text{Zr}_{0.25}\text{H}_{10}$	2.34	276	210
	$\text{La}_{0.75}\text{Ba}_{0.25}\text{H}_{10}$	2.34	269	178
	$\text{La}_{0.75}\text{Ce}_{0.25}\text{H}_{10}$	1.07	150	125

170

171 In Fig. 3(a), we found that substitution with Y, Sr, Lu, Hf, Zr, and Ba all enhance the EPC constant
172 and T_c at 400 GPa, while the substitution with Ce weakens them. Similarly, at 250 GPa, λ and T_c
173 increase with Y substitution while decreasing with Ce substitution. At 200 GPa, the only stable phase
174 $\text{La}_{0.75}\text{Ce}_{0.25}\text{H}_{10}$ remains a potential high- T_c superconductor with T_c of 246 K and λ of 3.08.



175

176

177

Fig. 3. Superconducting transition temperature (T_c) with and electron-phonon coupling constant λ of stable $\text{La}_{0.75}\text{M}_{0.25}\text{H}_{10}$ structures at (a) 400GPa, (b) 250GPa and (c) 200GPa

178

179

180

181

182

183

184

185

186

187

188

189

190

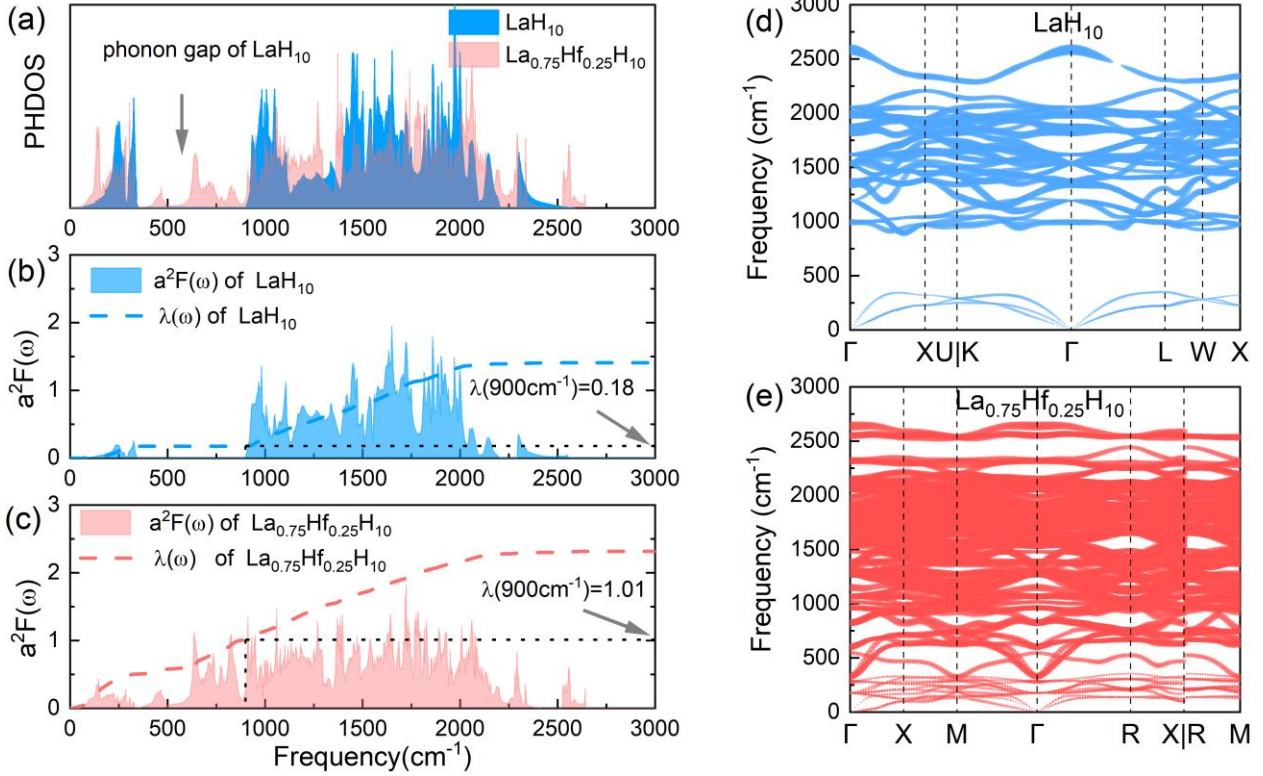
191

192

193

194

To understand the origin of the increased λ and T_c by doping, we use $\text{La}_{0.75}\text{Hf}_{0.25}\text{H}_{10}$ as an example and compare its phonon spectra to the LaH_{10} in Fig. 4. We find the substitution of La with Hf induces significant softening of high-frequency phonon modes. As shown in Fig. 4(a), with the Hf substitution, a few phonon modes appear in the low-frequency range of $360\text{-}900\text{ cm}^{-1}$, while no phonon modes exist in the same area for LaH_{10} . The H atoms dominate these phonon modes (see the projected phonon DOS in Fig. S7 [46]). Comparing the Eliashberg spectral function between LaH_{10} and $\text{La}_{0.75}\text{Hf}_{0.25}\text{H}_{10}$ in Fig. 4 (b) and (c), one can see the phonon softening at the range of $360\text{-}900\text{ cm}^{-1}$ significantly promotes the EPC in this region. Similar enhancement of phonon linewidth in $360\text{-}900\text{ cm}^{-1}$ can be found by comparing Fig. 4 (d) and (e). If we integrate Eq. (3) to $\omega = 900\text{ cm}^{-1}$, we find the contribution to λ from frequencies less than 900 cm^{-1} is 0.18 and 1.01 for LaH_{10} and $\text{La}_{0.75}\text{Hf}_{0.25}\text{H}_{10}$, respectively. Therefore, the phonon softening in $\text{La}_{0.75}\text{Hf}_{0.25}\text{H}_{10}$ significantly enhances the EPC. This mechanism is also seen in other superconducting systems [61-64]. The analysis of $\text{La}_{0.75}\text{Hf}_{0.25}\text{H}_{10}$ illustrates that substituting La with Hf changes the bonding with H atoms and softens vibrational modes. Such phonon softening enhances the EPC and increases the λ and T_c , simultaneously. We also analyzed the EPC for other dopants and found similar effects, as shown in Fig. S8 and Table S2 [46], i.e., the substitution of La leads to phonon softening, which contributes to strong EPC in the middle- and low-frequency regions.



195

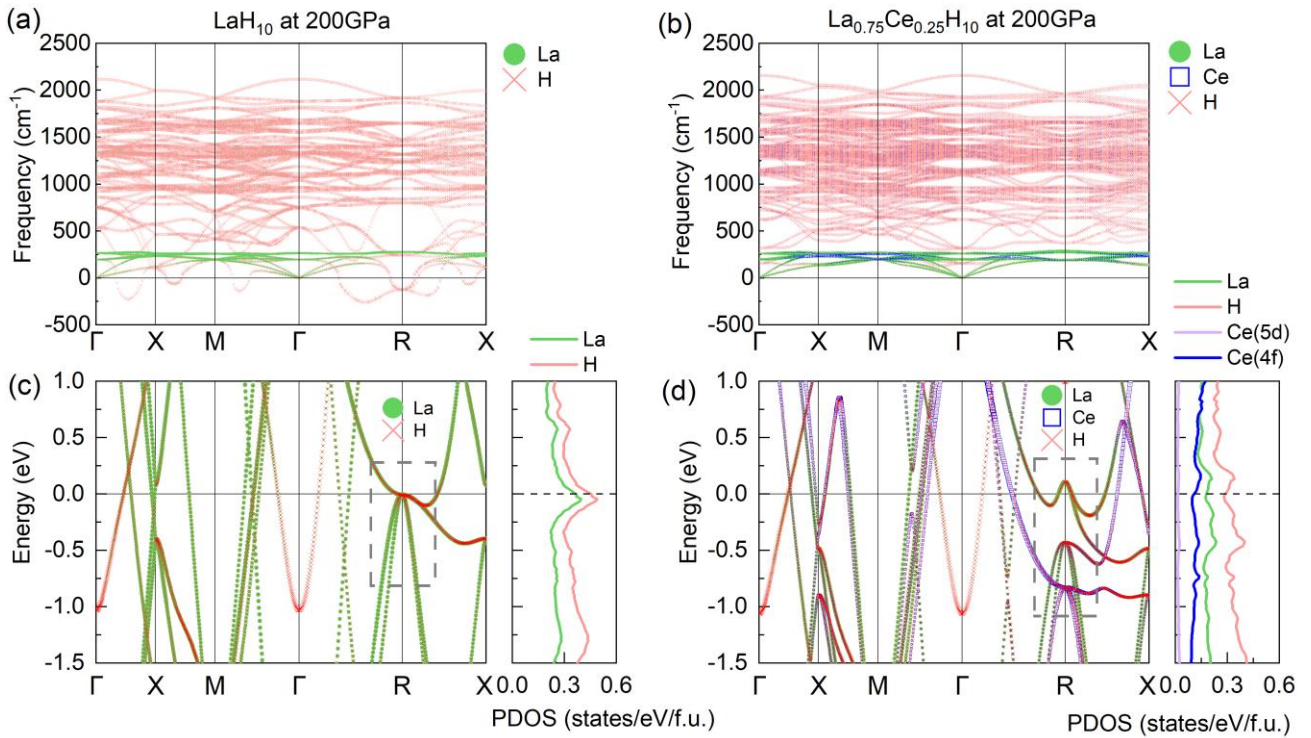
196 Fig. 4. (a) phonon dos of LaH_{10} and $\text{La}_{0.75}\text{Hf}_{0.25}\text{H}_{10}$ at 400GPa. (b) and (c) Eliashberg spectrum function
 197 $\alpha^2F(\omega)$, and electron-phonon coupling integral $\lambda(\omega)$ of LaH_{10} and $\text{La}_{0.75}\text{Hf}_{0.25}\text{H}_{10}$ at 400GPa. (d)
 198 and (e) Phonon spectrum of LaH_{10} and $\text{La}_{0.75}\text{Hf}_{0.25}\text{H}_{10}$ at 400GPa. The solid circles show the EPC with
 199 the area proportional to the respective phonon linewidth.

200 3.3 The effects of Ce

201 Ce is the only substitution that increases the pressure range of LaH_{10} stability while maintaining
 202 the high-temperature superconductivity with a slight weakening of the EPC in the harmonic
 203 approximation. To understand the effect of Ce substitution on dynamic stability, we compare the
 204 phonon spectrum between LaH_{10} and $\text{La}_{0.75}\text{Ce}_{0.25}\text{H}_{10}$ at 200 GPa in Fig. 5(a) and (b). In LaH_{10} , the
 205 imaginary frequency modes on the Γ -X, Γ -M, and Γ -R paths are dominated by the vibrations of
 206 hydrogen atoms. When Ce is introduced, these modes become stiffer, and the imaginary frequency
 207 disappears. In Fig. 5(c) and (d), we compare the electronic band structure and density of states for
 208 LaH_{10} and $\text{La}_{0.75}\text{Ce}_{0.25}\text{H}_{10}$, respectively. LaH_{10} shows a flat band near the Fermi level with eightfold
 209 degeneracy at the **R** point. This caused a Van Hove singularity (VHS) in the density of states. Ce
 210 substitution opens the gap at **R** and splits the degenerated bands. This removes the VHS and reduces
 211 the states at the Fermi level. Correspondingly, the imaginary modes at **R** disappear.

212 Moreover, additional bands contributed mainly by Ce and H cross the Fermi level at Γ -M and Γ -

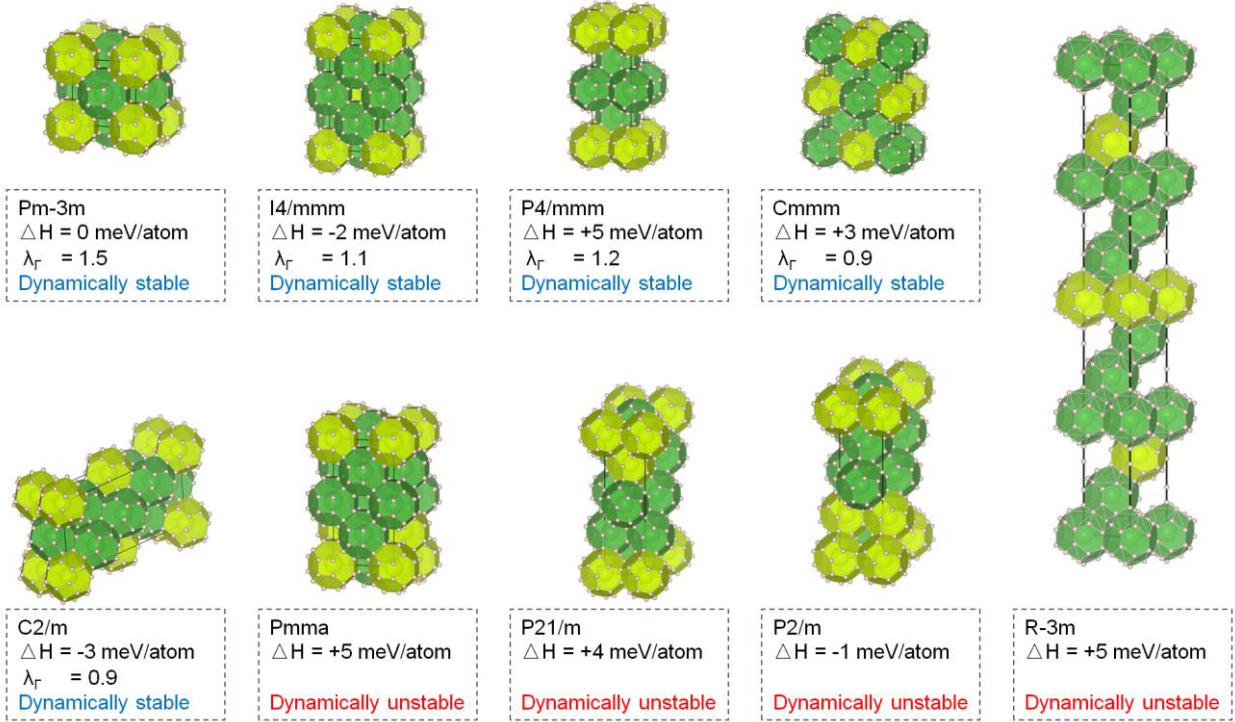
213 R paths in $\text{La}_{0.75}\text{Ce}_{0.25}\text{H}_{10}$. The bonding likely contributes to the hardening of phonon modes. Based
 214 on the electronic density of states, these Ce bands near the Fermi level are mostly from 4*f* orbitals.
 215 Therefore, this indicates that the 4*f* electron in Ce contributes significantly to the dynamic stability of
 216 $\text{La}_{0.75}\text{Ce}_{0.25}\text{H}_{10}$. To further validate this mechanism, we computed the phonon spectrum of
 217 $\text{La}_{0.75}\text{Ce}_{0.25}\text{H}_{10}$ with the ultrasoft pseudopotential where Ce's 4*f* electrons are regarded as core electrons.
 218 This ultrasoft pseudopotential leads to charge transfer and the re-appearance of imaginary modes
 219 caused by the Ce-4*f* electron as discussed in Supplementary Note 3 [46]. The results suggest the strong
 220 effect of Ce-4*f* electrons in stabilizing the LaH_{10} at low pressures.



221
 222 Fig. 5. (a) (b) Atom-projected phonon spectrum of LaH_{10} and $\text{La}_{0.75}\text{Ce}_{0.25}\text{H}_{10}$ at 200GPa. (c) (d) fat
 223 electron band (and projected density of states, PDOS) of LaH_{10} and $\text{La}_{0.75}\text{Ce}_{0.25}\text{H}_{10}$ at 200GPa.

224 So far, the substitutional effect of Ce was only considered with Pm-3m $\text{La}_{0.75}\text{Ce}_{0.25}\text{H}_{10}$ structure.
 225 We further examine the stability of other $\text{La}_{0.75}\text{Ce}_{0.25}\text{H}_{10}$ polymorphs at 200 GPa. As shown in Fig. 6,
 226 we construct LaH_{10} supercells (88 atoms) by $2 \times 2 \times 2$, $1 \times 1 \times 8$ and $1 \times 2 \times 4$ and randomly
 227 replace La atoms with Ce atoms to generate 9 unique structures. Energy calculations show that these
 228 structures all have similar enthalpy with differences less than 8 meV/atom. Harmonic phonon
 229 calculations shown in Fig. S9 [46] suggest five phases are dynamically stable, which is noted in Fig.
 230 6. To explore the possible superconductivity in these structures, we employ a recently developed
 231 frozen-phonon method to compute the zone-center EPC strength for stable structures. This efficient

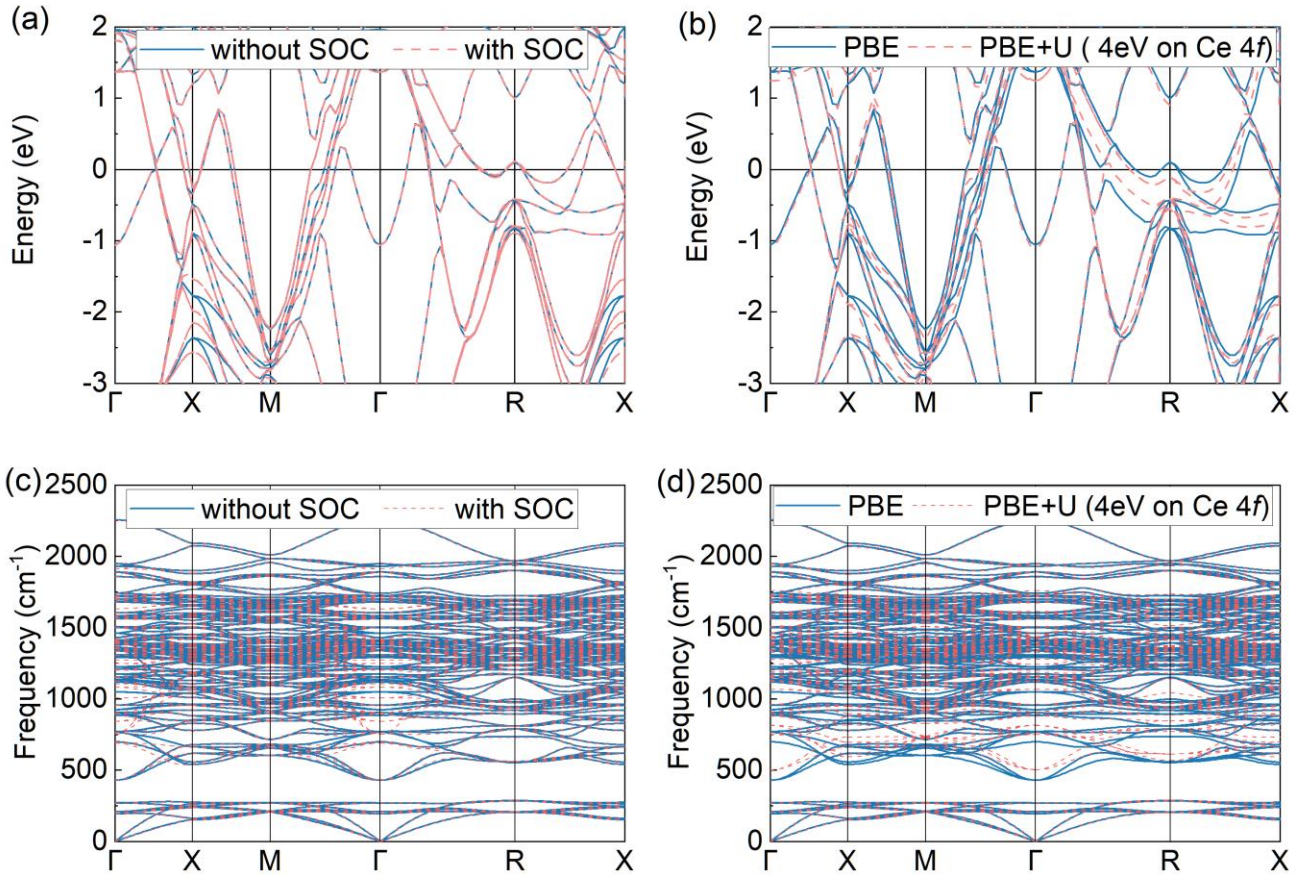
232 method can identify strong EPC candidates in hydrides because the zone-center EPC strongly
 233 correlates with the full Brillouin zone EPC in these materials [65]. Using this method, we compute the
 234 zone-center EPC, λ_{Γ} , for 5 dynamically stable polymorphs. As shown in Fig. 6, different structures
 235 show similar λ_{Γ} as the one of the Pm-3m phase. Therefore, Ce occupation in the $\text{La}_{0.75}\text{Ce}_{0.25}\text{H}_{10}$ does
 236 not affect its energetic stability and EPC. To confirm the zone-center EPC calculations, we also
 237 performed DFPT calculations of full Brillouin zone EPC for the P4/mmm phase (see details in Fig.
 238 S10 [46]). We obtained λ of P4/mmm as 2.64, slightly smaller than the Pm-3m phase ($\lambda=3.08$). This
 239 is consistent with the zone-center EPC calculations. The T_c was estimated 215K (with ME approach)
 240 at 200GPa, which is slightly smaller than the one of Pm-3m phase (246K). Since these polymorphs
 241 have similar energy, they may form a random solid solution in the experimental synthesis. Nevertheless,
 242 such a mixture should maintain the HTS because of the similar electron-phonon coupling strength in
 243 these phases.



244
 245 Fig. 6. The crystal structure, relative enthalpy ΔH and zone-center EPC λ_{Γ} of 9 $\text{La}_{0.75}\text{Ce}_{0.25}\text{H}_{10}$
 246 polymorphs at 200GPa. The green (yellow) polyhedron represents La-H (Ce-H) cages.

247 Additional effects such as spin-orbit coupling (SOC) and electron correlation of f -electron in Ce
 248 may affect the superconductivity of $\text{La}_{0.75}\text{Ce}_{0.25}\text{H}_{10}$. However, calculating the EPC and T_c directly
 249 under these effects is highly complex and sophisticated. Therefore, we performed additional SOC and
 250 DFT+U calculations to understand their effect on the electronic band structure and phonon dispersion

251 spectrum instead of direct calculations of EPC. Here, we choose the U (Ce-4*f*) value of 4 eV [66] for
 252 the PBE+ U calculation. As shown in Fig. 7, both SOC and DFT+ U calculations result in electronic
 253 and phonon band structures similar to the one without these effects. Therefore, we expect these effects
 254 should be weak on the EPC of $\text{La}_{0.75}\text{Ce}_{0.25}\text{H}_{10}$.



255

256 Fig. 7 (a) (b) Electron band structure of $\text{La}_{0.75}\text{Ce}_{0.25}\text{H}_{10}$ with or without SOC or U effects. (c) (d)
 257 phonon spectrum, respectively.

258 □. CONCLUSIONS

259 In summary, based on first-principles calculations, we have investigated the effects of chemical
 260 doping on phase stability and superconductivity in the LaH_{10} structure. By analyzing the phonon
 261 spectrum, we demonstrated that most doping elements (K, Rb, Cs, Ca, Sr, Ba, Sc, Y, Ti, Zr, Hf, Lu, In,
 262 Tl) induce the softening of the high-frequency phonon modes, thereby enhancing the EPC and
 263 improving T_c . However, phonon softening also leads to dynamical instability, reducing the stable
 264 pressure range. Unlike these dopants, Ce doping can expand the range of dynamical stability for LaH_{10}
 265 at lower pressures. The analysis of the electronic structures revealed that Ce doping eliminates the

266 VHS and reduces states at the Fermi level, stiffening a few imaginary modes in LaH₁₀ at low pressures.
267 Utilizing the Eliashberg theory, we demonstrated that La_{0.75}Ce_{0.25}H₁₀ maintains high-temperature
268 superconductivity with a T_c of ~ 246 K at 200GPa. Upon examining different polymorphs of
269 La_{0.75}Ce_{0.25}H₁₀, we show that different doping sites of Ce in the LaH₁₀ structure have a minor effect on
270 the energetic stability and EPC. Our findings suggest Ce can be a promising dopant to stabilize LaH₁₀
271 at lower pressures while preserving its high-temperature superconductivity. The experimental
272 verification of our prediction is highly desirable.

273

274 **Acknowledgments**

275 Y.S. acknowledges support from the Fundamental Research Funds for the Central Universities
276 (20720230014). V.P. was supported by the U.S. Department of Energy, Office of Basic Energy
277 Sciences, Division of Materials Sciences and Engineering. Ames National Laboratory is operated for
278 the U.S. Department of Energy by Iowa State University under Contract No. DE-AC02-07CH11358.
279 K.M.H. acknowledges support from National Science Foundation Awards No. DMR-2132666. A.P.D.
280 acknowledges financial support from the National Science Centre (Poland) under project No.
281 2022/47/B/ST3/0062. S. Fang and T. Wu from the Information and Network Center of Xiamen
282 University are acknowledged for their help with GPU computing. Tan Kah Kee Supercomputing
283 Center is acknowledged for its support of high-performance computing.

284

285 **Reference**

- 286 [1] A. P. Drozdov, M. I. Eremets, I. A. Troyan, V. Ksenofontov, and S. I. Shylin, Conventional
287 superconductivity at 203 kelvin at high pressures in the sulfur hydride system, *Nature* **525**, 73 (2015).
288 [2] A. P. Drozdov, P. P. Kong, V. S. Minkov, M. Tkacz, and M. I. Eremets, Superconductivity at 250 K in
289 lanthanum hydride under high pressures, *Nature* **569**, 528 (2019).
290 [3] M. Somayazulu, M. Ahart, A. K. Mishra, Z. M. Geballe, M. Baldini, Y. Meng, V. V. Struzhkin, and R. J.
291 Hemley, Evidence for Superconductivity above 260 K in Lanthanum Superhydride at Megabar Pressures, *Phys.*
292 *Rev. Lett.* **122**, 027001 (2019).
293 [4] Z. Li, X. He, C. Zhang, X. Wang, S. Zhang, Y. Jia, S. Feng, K. Lu, J. Zhao, J. Zhang, B. Min, Y. Long, R.
294 Yu, L. Wang, M. Ye, Z. Zhang, V. Prakapenka, S. Chariton, P. A. Ginsberg, J. Bass, S. Yuan, H. Liu, and C. Jin,
295 Superconductivity above 200 K discovered in superhydrides of calcium, *Nat. Commun.* **13**, 2863 (2022).
296 [5] L. Ma, K. Wang, Y. Xie, X. Yang, Y. Wang, M. Zhou, H. Liu, X. Yu, Y. Zhao, H. Wang, G. Liu, and Y. Ma,
297 High-Temperature Superconducting Phase in Clathrate Calcium Hydride CaH₆ up to 215 K at a Pressure of
298 172 GPa, *Phys. Rev. Lett.* **128**, 167001 (2022).
299 [6] W. Chen, D. V. Semenok, X. Huang, H. Shu, X. Li, D. Duan, T. Cui, and A. R. Oganov, High-Temperature
300 Superconducting Phases in Cerium Superhydride with a T_c up to 115 K below a Pressure of 1 Megabar, *Phys.*
301 *Rev. Lett.* **127**, 117001 (2021).
302 [7] J. Bi, Y. Nakamoto, P. Zhang, K. Shimizu, B. Zou, H. Liu, M. Zhou, G. Liu, H. Wang, and Y. Ma, Giant

303 enhancement of superconducting critical temperature in substitutional alloy (La,Ce)H(9), *Nat. Commun.* **13**,
304 5952 (2022).

305 [8] W. Chen, X. Huang, D. V. Semenov, S. Chen, D. Zhou, K. Zhang, A. R. Oganov, and T. Cui, Enhancement
306 of superconducting properties in the La-Ce-H system at moderate pressures, *Nat. Commun.* **14**, 2660 (2023).

307 [9] P. Kong, V. S. Minkov, M. A. Kuzovnikov, A. P. Drozdov, S. P. Besedin, S. Mozaffari, L. Balicas, F. F.
308 Balakirev, V. B. Prakapenka, S. Chariton, D. A. Knyazev, E. Greenberg, and M. I. Eremets, Superconductivity
309 up to 243 K in the yttrium-hydrogen system under high pressure, *Nat. Commun.* **12**, 5075 (2021).

310 [10] E. Snider, N. Dasenbrock-Gammon, R. McBride, X. Wang, N. Meyers, K. V. Lawler, E. Zurek, A. Salamat,
311 and R. P. Dias, Synthesis of Yttrium Superhydride Superconductor with a Transition Temperature up to 262 K
312 by Catalytic Hydrogenation at High Pressures, *Phys. Rev. Lett.* **126**, 117003 (2021).

313 [11] Y. Wang, K. Wang, Y. Sun, L. Ma, Y. Wang, B. Zou, G. Liu, M. Zhou, and H. Wang, Synthesis and
314 superconductivity in yttrium superhydrides under high pressure, *Chin. Phys. B* **31**, 106201 (2022).

315 [12] D. V. Semenov, I. A. Troyan, A. G. Ivanova, A. G. Kvashnin, I. A. Kruglov, M. Hanfland, A. V. Sadakov,
316 O. A. Sobolevskiy, K. S. Pervakov, I. S. Lyubutin, K. V. Glazyrin, N. Giordano, D. N. Karimov, A. L. Vasiliev,
317 R. Akashi, V. M. Pudalov, and A. R. Oganov, Superconductivity at 253 K in lanthanum–yttrium ternary hydrides,
318 *Materials Today* **48**, 18 (2021).

319 [13] Y. Song, J. Bi, Y. Nakamoto, K. Shimizu, H. Liu, B. Zou, G. Liu, H. Wang, and Y. Ma, Stoichiometric
320 Ternary Superhydride LaBeH₈ as a New Template for High-Temperature Superconductivity at 110 K under 80
321 GPa, *Phys. Rev. Lett.* **130**, 266001 (2023).

322 [14] J. A. Flores-Livas, L. Boeri, A. Sanna, G. Profeta, R. Arita, and M. Eremets, A perspective on conventional
323 high-temperature superconductors at high pressure: Methods and materials, *Phys. Rep.* **856**, 1 (2020).

324 [15] L. P. Gor'kov and V. Z. Kresin, Colloquium: High pressure and road to room temperature superconductivity,
325 *Rev. Mod. Phys.* **90**, 011001 (2018).

326 [16] B. Lilia, R. Hennig, P. Hirschfeld, G. Profeta, A. Sanna, E. Zurek, W. E. Pickett, M. Amsler, R. Dias, M. I.
327 Eremets, C. Heil, R. J. Hemley, H. Liu, Y. Ma, C. Pierleoni, A. N. Kolmogorov, N. Rybin, D. Novoselov, V.
328 Anisimov, A. R. Oganov, C. J. Pickard, T. Bi, R. Arita, I. Errea, C. Pellegrini, R. Requist, E. K. U. Gross, E. R.
329 Margine, S. R. Xie, Y. Quan, A. Hire, L. Fanfarillo, G. R. Stewart, J. J. Hamlin, V. Stanev, R. S. Gonnelli, E.
330 Piatti, D. Romanin, D. Daghero, and R. Valenti, The 2021 room-temperature superconductivity roadmap, *J.*
331 *Phys. Condens. Matter* **34**, 183002 (2022).

332 [17] C. J. Pickard, I. Errea, and M. I. Eremets, Superconducting Hydrides Under Pressure, *Annu. Rev. Condens.*
333 *Matter Phys.* **11**, 57 (2020).

334 [18] W. E. Pickett, Colloquium: Room temperature superconductivity: The roles of theory and materials design,
335 *Rev. Mod. Phys.* **95**, 021001 (2023).

336 [19] Y. Sun, H.-Y. Liu, and Y.-M. Ma, Progress on hydrogen-rich superconductors under high pressure, *Acta*
337 *Physica Sinica* **70**, 017407 (2021).

338 [20] M. Du, W. Zhao, T. Cui, and D. Duan, Compressed superhydrides: the road to room temperature
339 superconductivity, *J Phys Condens Matter* **34**, 173001 (2022).

340 [21] D. V. Semenov, I. A. Kruglov, I. A. Savkin, A. G. Kvashnin, and A. R. Oganov, On Distribution of
341 Superconductivity in Metal Hydrides, *Curr. Opin. Solid State Mater. Sci.* **24**, 100808 (2020).

342 [22] X. Zhang, Y. Zhao, and G. Yang, Superconducting ternary hydrides under high pressure, *Wiley*
343 *Interdisciplinary Reviews: Computational Molecular Science* **12**, e1582 (2021).

344 [23] Z. Zhang, T. Cui, M. J. Hutcheon, A. M. Shipley, H. Song, M. Du, V. Z. Kresin, D. Duan, C. J. Pickard,
345 and Y. Yao, Design Principles for High-Temperature Superconductors with a Hydrogen-Based Alloy Backbone

346 at Moderate Pressure, *Phys. Rev. Lett.* **128**, 047001 (2022).

347 [24] M. Gao, X.-W. Yan, Z.-Y. Lu, and T. Xiang, Phonon-mediated high-temperature superconductivity in the
348 ternary borohydride KB₂H₈ under pressure near 12 GPa, *Phys. Rev. B* **104**, L100504 (2021).

349 [25] S. Di Cataldo, W. von der Linden, and L. Boeri, First-principles search of hot superconductivity in La-X-
350 H ternary hydrides, *npj Comput. Mater* **8**, 2 (2022).

351 [26] S. Di Cataldo, C. Heil, W. von der Linden, and L. Boeri, LaBH₈: Towards high-T_c low-pressure
352 superconductivity in ternary superhydrides, *Phys. Rev. B* **104**, L020511 (2021).

353 [27] N. Geng, K. P. Hilleke, L. Zhu, X. Wang, T. A. Strobel, and E. Zurek, Conventional High-Temperature
354 Superconductivity in Metallic, Covalently Bonded, Binary-Guest C-B Clathrates, *J. Am. Chem. Soc.* **145**, 1696
355 (2023).

356 [28] Y. Hai, H. Tian, M. Jiang, W. Li, G. Zhong, C. Yang, X. Chen, and H. Lin, Improving T_c in sodalite-like
357 boron-nitrogen compound M₂(BN)₆, *Mater. Today Phys.* **25**, 100699 (2022).

358 [29] R. Wang, Y. Sun, S. Wu, V. Antropov, and K. M. Ho, High-Throughput Screening of Strong Electron-
359 Phonon Couplings in Ternary Metal Diborides, *Inorg. Chem* **61**, 18154 (2022).

360 [30] M. Du, H. Song, Z. Zhang, D. Duan, and T. Cui, Room-Temperature Superconductivity in Yb/Lu
361 Substituted Clathrate Hexahydrides under Moderate Pressure, *Research* **2022**, 9784309 (2022).

362 [31] Y.-L. Hai, H.-L. Tian, M.-J. Jiang, H.-B. Ding, Y.-J. Feng, G.-H. Zhong, C.-L. Yang, X.-J. Chen, and H.-Q.
363 Lin, Prediction of high-T_c superconductivity in H₆SX(X=Cl,Br) at pressures below one megabar, *Phys. Rev. B*
364 **105**, L180508 (2022).

365 [32] M.-J. Jiang, Y.-L. Hai, H.-L. Tian, H.-B. Ding, Y.-J. Feng, C.-L. Yang, X.-J. Chen, and G.-H. Zhong, High-
366 temperature superconductivity below 100GPa in ternary C-based hydride MC₂H₈ with molecular crystal
367 characteristics (M= Na, K, Mg, Al, and Ga), *Phys. Rev. B* **105**, 104511 (2022).

368 [33] T. Wang, J. A. Flores-Livas, T. Nomoto, Y. Ma, T. Koretsune, and R. Arita, Optimal alloying in hydrides:
369 Reaching room-temperature superconductivity in LaH₁₀, *Phys. Rev. B* **105**, 174516 (2022).

370 [34] H. Song, Z. Zhang, T. Cui, C. J. Pickard, V. Z. Kresin, and D. Duan, High T_c Superconductivity in Heavy
371 Rare Earth Hydrides, *Chin. Phys. Lett.* **38**, 107401 (2021).

372 [35] X. Zhong, Y. Sun, T. Iitaka, M. Xu, H. Liu, R. J. Hemley, C. Chen, and Y. Ma, Prediction of Above-Room-
373 Temperature Superconductivity in Lanthanide/Actinide Extreme Superhydrides, *J. Am. Chem. Soc.* **144**, 13394
374 (2022).

375 [36] J. P. Perdew, K. Burke, and M. Ernzerhof, Generalized gradient approximation made simple, *Phys. Rev.*
376 *Lett.* **77**, 3865 (1996).

377 [37] P. E. Blochl, Projector augmented-wave method, *Phys. Rev. B* **50**, 17953 (1994).

378 [38] G. Kresse and J. Furthmüller, Efficient iterative schemes for ab initio total-energy calculations using a
379 plane-wave basis set, *Phys. Rev. B* **54**, 11169 (1996).

380 [39] A. Togo, L. Chaput, T. Tadano, and I. Tanaka, Implementation strategies in phonopy and phono3py, *J Phys*
381 *Condens Matter* **35**, 353001(2023).

382 [40] S. Baroni, S. De Gironcoli, A. Dal Corso, and P. Giannozzi, Phonons and related crystal properties from
383 density-functional perturbation theory, *Rev. Mod. Phys.* **73**, 515 (2001).

384 [41] P. Giannozzi, O. Andreussi, T. Brumme, O. Bunau, M. Buongiorno Nardelli, M. Calandra, R. Car, C.
385 Cavazzoni, D. Ceresoli, M. Cococcioni, N. Colonna, I. Carnimeo, A. Dal Corso, S. de Gironcoli, P. Delugas, R.
386 A. DiStasio, Jr., A. Ferretti, A. Floris, G. Fratesi, G. Fugallo, R. Gebauer, U. Gerstmann, F. Giustino, T. Gorni,
387 J. Jia, M. Kawamura, H. Y. Ko, A. Kokalj, E. Kucukbenli, M. Lazzeri, M. Marsili, N. Marzari, F. Mauri, N. L.
388 Nguyen, H. V. Nguyen, A. Otero-de-la-Roza, L. Paulatto, S. Ponce, D. Rocca, R. Sabatini, B. Santra, M. Schlipf,

389 A. P. Seitsonen, A. Smogunov, I. Timrov, T. Thonhauser, P. Umari, N. Vast, X. Wu, and S. Baroni, Advanced
390 capabilities for materials modelling with Quantum ESPRESSO, *J. Phys. Condens. Matter* **29**, 465901 (2017).

391 [42] P. Giannozzi, S. Baroni, N. Bonini, M. Calandra, R. Car, C. Cavazzoni, D. Ceresoli, G. L. Chiarotti, M.
392 Cococcioni, I. Dabo, A. Dal Corso, S. de Gironcoli, S. Fabris, G. Fratesi, R. Gebauer, U. Gerstmann, C.
393 Gougoussis, A. Kokalj, M. Lazzeri, L. Martin-Samos, N. Marzari, F. Mauri, R. Mazzarello, S. Paolini, A.
394 Pasquarello, L. Paulatto, C. Sbraccia, S. Scandolo, G. Sclauzero, A. P. Seitsonen, A. Smogunov, P. Umari, and
395 R. M. Wentzcovitch, QUANTUM ESPRESSO: a modular and open-source software project for quantum
396 simulations of materials, *J. Phys. Condens. Matter* **21**, 395502 (2009).

397 [43] A. Dal Corso, Pseudopotentials periodic table: From H to Pu, *Comput. Mater. Sci.* **95**, 337 (2014).

398 [44] P. B. Allen and R. C. Dynes, Transition temperature of strong-coupled superconductors reanalyzed, *Phys.*
399 *Rev. B* **12**, 905 (1975).

400 [45] W. L. McMillan, Transition Temperature of Strong-Coupled Superconductors, *Phys. Rev.* **167**, 331 (1968).

401 [46] See Supplemental Material at <http://link.aps.org/supplemental/xxxxxxx> for convergence test of electron-
402 phonon coupling calculations, finite-temperature thermodynamic stability, effect of $4f$ electron, additional
403 phonon spectrum and more calculation details, which includes Refs. [47, 67-73].

404 [47] H. Liu, Naumov, II, R. Hoffmann, N. W. Ashcroft, and R. J. Hemley, Potential high-T(c) superconducting
405 lanthanum and yttrium hydrides at high pressure, *Proc. Natl. Acad. Sci. U.S.A.* **114**, 6990 (2017).

406 [48] P. Morel and P. W. Anderson, Calculation of the Superconducting State Parameters with Retarded Electron-
407 Phonon Interaction, *Phys. Rev.* **125**, 1263 (1962).

408 [49] G. Eliashberg, Interactions between electrons and lattice vibrations in a superconductor, *Sov. Phys. JETP*
409 **11**, 696 (1960).

410 [50] F. Marsiglio, M. Schossmann, and J. Carbotte, Iterative analytic continuation of the electron self-energy to
411 the real axis, *Phys. Rev. B* **37**, 4965 (1988).

412 [51] A. P. Durajski and R. Szcześniak, New superconducting superhydride LaC₂H₈ at relatively low
413 stabilization pressure, *Physical Chemistry Chemical Physics* **23**, 25070 (2021).

414 [52] A. P. Durajski, R. Szcześniak, Y. Li, C. Wang, and J.-H. Cho, Isotope effect in superconducting lanthanum
415 hydride under high compression, *Phys. Rev. B* **101**, 214501 (2020).

416 [53] R. Szcześniak, The numerical solution of the imaginary-axis Eliashberg equations, *Acta Physica Polonica*
417 **A 109**, 179 (2006).

418 [54] I. Errea, F. Belli, L. Monacelli, A. Sanna, T. Koretsune, F. Mauri, and J. A. Flores-Livas, Quantum crystal
419 structure in the 250-kelvin superconducting lanthanum hydride, *Nature* **578**, 66 (2020).

420 [55] I. Errea, M. Calandra, C. J. Pickard, J. R. Nelson, R. J. Needs, Y. Li, H. Liu, Y. Zhang, Y. Ma, and F. Mauri,
421 Quantum hydrogen-bond symmetrization in the superconducting hydrogen sulfide system, *Nature* **532**, 81
422 (2016).

423 [56] P. Hou, F. Belli, R. Bianco, and I. Errea, Quantum anharmonic enhancement of superconductivity in
424 P63/mmc ScH₆ at high pressures: A first-principles study, *J. Appl. Phys.* **130**, 175902 (2021).

425 [57] I. A. Troyan, D. V. Semenok, A. G. Kvashnin, A. V. Sadakov, O. A. Sobolevskiy, V. M. Pudalov, A. G.
426 Ivanova, V. B. Prakapenka, E. Greenberg, A. G. Gavriluk, I. S. Lyubutin, V. V. Struzhkin, A. Bergara, I. Errea,
427 R. Bianco, M. Calandra, F. Mauri, L. Monacelli, R. Akashi, and A. R. Oganov, Anomalous High-Temperature
428 Superconductivity in YH₆, *Adv Mater* **33**, e2006832 (2021).

429 [58] H. Liu, I. I. Naumov, Z. M. Geballe, M. Somayazulu, J. S. Tse, and R. J. Hemley, Dynamics and
430 superconductivity in compressed lanthanum superhydride, *Phys. Rev. B* **98**, 100102 (2018).

431 [59] D. Sun, V. S. Minkov, S. Mozaffari, L. Balicas, and F. F. Balakirev, High-temperature superconductivity

432 on the verge of a structural instability in lanthanum superhydride, *Nat. Commun.* **12**, 6863 (2021).
433 [60] A. Durajski, R. Szcześniak, and L. Pietronero, High-temperature study of superconducting hydrogen and
434 deuterium sulfide, *Annalen der Physik* **528**, 358 (2016).
435 [61] P. B. Allen and M. L. Cohen, Superconductivity and Phonon Softening, *Phys. Rev. Lett.* **29**, 1593 (1972).
436 [62] P. B. Allen and R. C. Dynes, Superconductivity and phonon softening: II. Lead alloys, *Phys. Rev. B* **11**,
437 1895 (1975).
438 [63] K. Kudo, M. Takasuga, Y. Okamoto, Z. Hiroi, and M. Nohara, Giant phonon softening and enhancement
439 of superconductivity by phosphorus doping of BaNi₂As₂, *Phys. Rev. Lett.* **109**, 097002 (2012).
440 [64] W. E. Pickett and P. B. Allen, Superconductivity and phonon softening. III. Relation between electron bands
441 and phonons in Nb, Mo, and their alloys, *Phys. Rev. B* **16**, 3127 (1977).
442 [65] Y. Sun, F. Zhang, C.-Z. Wang, K.-M. Ho, I. I. Mazin, and V. Antropov, Electron-phonon coupling strength
443 from ab initio frozen-phonon approach, *Phys. Rev. Mater.* **6**, 074801 (2022).
444 [66] B. Y. Ao, X. L. Wang, P. Shi, P. H. Chen, X. Q. Ye, X. C. Lai, J. J. Ai, and T. Gao, Lattice contraction of
445 cerium hydrides from first-principles LDA+U calculations, *International Journal of Hydrogen Energy* **37**, 5108
446 (2012).
447 [67] M. Gao, Q.-Z. Li, X.-W. Yan, and J. Wang, Prediction of phonon-mediated superconductivity in borophene,
448 *Phys. Rev. B* **95**, 024505 (2017).
449 [68] F. Peng, Y. Sun, C. J. Pickard, R. J. Needs, Q. Wu, and Y. Ma, Hydrogen Clathrate Structures in Rare Earth
450 Hydrides at High Pressures: Possible Route to Room-Temperature Superconductivity, *Phys. Rev. Lett.* **119**,
451 107001 (2017).
452 [69] C. J. Pickard and R. J. Needs, Structure of phase III of solid hydrogen, *Nature Physics* **3**, 473 (2007).
453 [70] N. P. Salke, M. M. Davari Esfahani, Y. Zhang, I. A. Kruglov, J. Zhou, Y. Wang, E. Greenberg, V. B.
454 Prakapenka, J. Liu, A. R. Oganov, and J. F. Lin, Synthesis of clathrate cerium superhydride CeH(9) at 80-100
455 GPa with atomic hydrogen sublattice, *Nat. Commun.* **10**, 4453 (2019).
456 [71] A. M. Shipley, M. J. Hutcheon, M. S. Johnson, R. J. Needs, and C. J. Pickard, Stability and
457 superconductivity of lanthanum and yttrium decahydrides, *Phys. Rev. B* **101**, 224511 (2020).
458 [72] P. Song, Z. Hou, K. Nakano, K. Hongo, and R. Maezono, Potential high-T_c superconductivity in YCeH
459 and LaCeH under pressure, *Mater. Today Phys.* **28**, 100873 (2022).
460 [73] M. Wierzbowska, S. de Gironcoli, and P. Giannozzi, Origins of low-and high-pressure discontinuities of
461 T_c in niobium, arXiv preprint cond-mat/0504077 (2005).
462
463